

Implications of PREX-II on the equation of state of neutron-rich matter

Brendan T. Reed,^{1,2,*} F. J. Fattoyev,^{3,†} C. J. Horowitz,^{2,‡} and J. Piekarewicz^{4,§}

¹*Department of Astronomy, Indiana University, Bloomington, Indiana 47405, USA*

²*Center for Exploration of Energy and Matter and Department of Physics, Indiana University, Bloomington, IN 47405, USA*

³*Department of Physics, Manhattan College, Riverdale, NY 10471, USA*

⁴*Department of Physics, Florida State University, Tallahassee, FL 32306, USA*

(Dated: April 2, 2021)

Laboratory experiments sensitive to the equation of state of neutron rich matter in the vicinity of nuclear saturation density provide the first rung in a “density ladder” that connects terrestrial experiments to astronomical observations. In this context, the neutron skin thickness of ^{208}Pb (R_{skin}^{208}) provides a stringent laboratory constraint on the density dependence of the symmetry energy. In turn, an improved value of R_{skin}^{208} has been reported recently by the PREX collaboration. Exploiting the strong correlation between R_{skin}^{208} and the slope of the symmetry energy L within a specific class of relativistic energy density functionals, we report a value of $L = (106 \pm 37)$ MeV—that systematically overestimates current limits based on both theoretical approaches and experimental measurements. The impact of such a stiff symmetry energy on some critical neutron-star observables is also examined.

PACS numbers: 21.60.Jz, 24.10.Jv, 26.60.Kp, 97.60.Jd

The updated Lead Radius EXperiment (PREX-II) has delivered on the promise to determine the neutron radius of ^{208}Pb with a precision of nearly 1%. By combining the original PREX result [1, 2] with the newly announced PREX-II measurement, the following value for the neutron skin thickness of ^{208}Pb was reported [3]:

$$R_{\text{skin}} = R_n - R_p = (0.283 \pm 0.071) \text{ fm}, \quad (1)$$

where the quoted uncertainty represents a 1σ error, and R_n and R_p are the root-mean-square radii of the neutron and proton density distributions, respectively. Such a purely electroweak measurement is of critical importance in constraining both models of nuclear structure as well as the equation of state (EOS) of neutron-rich matter in the vicinity of nuclear saturation density ($\rho_0 \approx 0.15 \text{ fm}^{-3}$). In turn, the EOS around saturation density provides the first rung in a “density ladder” that connects laboratory experiment to astronomical observations that probe the EOS at higher densities. It is the aim of this letter to explore the impact of PREX-II on certain parameters of the EOS that, in turn, dictates the behavior of several neutron-star observables.

For two decades the neutron skin thickness of ^{208}Pb has been identified as an ideal laboratory observable to constrain the EOS of neutron rich matter, particularly the poorly determined density dependence of the symmetry energy [4–7]. The EOS of infinite nuclear matter at zero temperature is enshrined in the energy per particle which depends on both the conserved neutron (ρ_n) and proton

(ρ_p) densities; here we assume that the electroweak sector has been “turned off”. Moreover, it is customary to separate the EOS into two contributions, one that represents the energy of symmetric ($\rho_n = \rho_p$) nuclear matter and another one that accounts for the breaking of the symmetry. That is,

$$\frac{E}{A}(\rho, \alpha) - M \equiv \mathcal{E}(\rho, \alpha) = \mathcal{E}_{\text{SNM}}(\rho) + \alpha^2 \mathcal{S}(\rho) + \mathcal{O}(\alpha^4), \quad (2)$$

where $\rho = (\rho_n + \rho_p)$ is the total baryon density given by the sum of neutron and proton densities, and $\alpha = (\rho_n - \rho_p)/\rho$ is the neutron-proton asymmetry. The first-order correction to the energy of symmetric nuclear matter $\mathcal{E}_{\text{SNM}}(\rho)$ is encoded in the symmetry energy $\mathcal{S}(\rho)$. The symmetry energy quantifies the increase in the energy per particle of infinite nuclear matter for systems with an isospin imbalance (e.g., more neutrons than protons). Further, given the preeminent role of nuclear saturation, the energy of symmetric nuclear matter and the symmetry energy may be described in terms of a few bulk parameters that characterize their behavior around saturation density. In this letter we focus on the density dependence of the symmetry energy [8]:

$$\mathcal{S}(\rho) = J + L \frac{(\rho - \rho_0)}{3\rho_0} + \dots \quad (3)$$

The first term (J) represents the correction to the binding energy of symmetric nuclear matter, whereas the second term (L) dictates how rapidly the symmetry energy increases with density. It is the slope of the symmetry energy L that displays a strong correlation to the neutron skin thickness of ^{208}Pb . Given that symmetric nuclear matter saturates, namely, its pressure vanishes at saturation, the slope of the symmetry energy L is closely related to the pressure of pure neutron matter at satura-

*Electronic address: reedbr@iu.edu

†Electronic address: ffattoyev01@manhattan.edu

‡Electronic address: horowitz@indiana.edu

§Electronic address: jpiekarewicz@fsu.edu

tion density. That is,

$$P_{\text{PNM}}(\rho_0) \approx \frac{1}{3} L \rho_0. \quad (4)$$

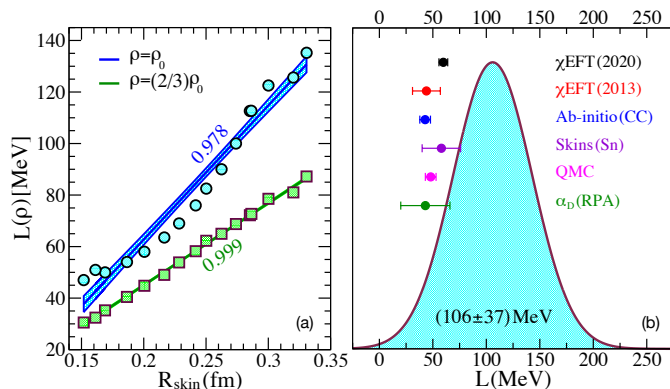


FIG. 1: (Color online) *Left*: Slope of the symmetry energy at nuclear saturation density ρ_0 (blue upper line) and at $(2/3)\rho_0$ (green lower line) as a function of R_{skin}^{208} . The numbers next to the lines denote values for the correlation coefficients. *Right*: Gaussian probability distribution for the slope of the symmetry energy $L = L(\rho_0)$ inferred by combining the linear correlation in the left figure with the recently reported PREX-II limit. The six error bars are constraints on L obtained by using different theoretical approaches [9–16].

To assess the impact of the combined PREX–PREX-II measurements (henceforth referred simply as “PREX-II”)—we provide predictions for several observables using a set of 16 covariant energy density functionals. These are FSUGold2 [17] together with a set of eight systematically varied interactions—FSUGold2–L047, L050, L054, L058, L069, L076, L090, L100—with identical isoscalar properties as FSUGold2, but isovector properties defined by the associated value of the slope of the symmetry energy L . For example, FSUGold2=FSUGold2–L113 predicts a slope of the symmetry energy of $L = 113$ MeV. Another set of accurately calibrated density functionals is given by RMF012, RMF016, RMF022, and RMF032 [18], where now the labels are associated to the predicted value of R_{skin}^{208} . For example, RMF032 predicts a neutron skin thickness of $R_{\text{skin}}^{208} = 0.32$ fm. Finally, TFa, TFb, and TFc, with $R_{\text{skin}}^{208} = 0.25, 0.30,$ and 0.33 fm, respectively, were created to test whether the large central value of $R_{\text{skin}}^{208} = 0.33$ fm originally reported by the PREX collaboration [1] was incompatible with other laboratory experiments and/or astrophysical observations [19]. We found then, that there was no compelling reason to rule out models with large neutron skins.

From the compilation of all these 16 models one obtains for the binding energy per nucleon and the charge radius of ^{208}Pb the following values: $B/A = 7.88 \pm 0.01$ MeV and $R_{\text{ch}} = 5.51 \pm 0.01$ fm, which compare well against the experimental values of $B/A = 7.87$ MeV and $R_{\text{ch}} = 5.50$ fm, respectively. A detailed description of the fitting protocol—including an explanation of the model and the

observables used in the calibration procedure—may be found in Refs. [17–19]. Moreover we underscore that the models considered here span a wide range of values for both the neutron skin thickness of ^{208}Pb and the associated slope of the symmetry energy. Indeed, the range of adopted values is almost as wide as the one used in the multi-model analysis of the sensitivity of the symmetry energy to the electric dipole polarizability and weak-charge form factor of both ^{48}Ca and ^{208}Pb [20, 21].

The strong correlation between L and R_{skin}^{208} in the context of the new PREX-II measurement is illustrated in Fig. 1. The left-hand panel displays the well-known correlation between the slope of the symmetry energy at saturation density and the neutron-skin thickness of ^{208}Pb . Also shown in Fig. 1(a) is the even stronger correlation between R_{skin} and the slope of the symmetry energy at the slightly lower density of $\tilde{\rho}_0 = (2/3)\rho_0 \approx 0.1 \text{ fm}^{-3}$ [5, 9, 22–25]. At such a lower density, which represents an average value between the central and surface densities, the symmetry energy is well constrained by the binding energy of heavy nuclei with a significant neutron excess. Relying on the strong $R_{\text{skin}}-L$ correlation together with the improved PREX-II limit, one obtains the gaussian probability distribution for L displayed in Fig. 1(b). Using the same analysis on both J and \tilde{L} —the latter representing the slope of the symmetry energy at $\tilde{\rho}_0$ —we derive the following limits:

$$J = (38.1 \pm 4.7) \text{ MeV}, \quad (5a)$$

$$L = (106 \pm 37) \text{ MeV}, \quad (5b)$$

$$\tilde{L} = (71.5 \pm 22.6) \text{ MeV}. \quad (5c)$$

As indicated in Fig. 1(b), these limits are systematically larger than those obtained using either purely theoretical approaches or extracted from a theoretical interpretation of experimental data [9–16]. We underscore that the models used in this letter represent a particular class of relativistic EDFs.

We note that theoretical interpretations of elastic nucleon-nucleus scattering cross sections together with quasielastic reactions to isobaric analog states obtained limits on L that are consistent with our findings [26]. The PREX-II result is also considerably larger—and in many cases incompatible—with experimental determinations of R_{skin}^{208} by methods that are highly model dependent [27–30]. A notable exception is the dispersive optical model analysis of the Washington University group that reported a neutron skin thickness of $R_{\text{skin}}^{208} = (0.25 \pm 0.05) \text{ fm}$ [31]; a revised lower value of $R_{\text{skin}}^{208} = (0.18 \pm 0.07) \text{ fm}$ —still consistent with [31]—was reported shortly thereafter in Ref. [32].

To further underscore the tension between PREX-II and our current understanding of the EOS, we display in Fig. 2 a summary of simultaneous constraints on both J and L as reported in Refs. [11, 33]. We have adapted Figure 2 from Ref. [11] by including the PREX-II limits on both J and L derived in Eq.(5). Note that with the exception of the analysis of Ref. [13], all other approaches

suggest a positive correlation between L and J . In the context of density functional theory, such a positive correlation is easy to understand. Using Eq.(3) at $\tilde{\rho}_0$ yields

$$S(\tilde{\rho}_0) = J - \frac{L}{9} \rightarrow J \approx \left(26 \text{ MeV} + \frac{L}{9} \right). \quad (6)$$

The value of $S(\tilde{\rho}_0) \approx 26 \text{ MeV}$ [22] follows because the symmetry energy at $\tilde{\rho}_0$ is tightly constrained by the binding energy of heavy nuclei. The PREX-II inferred value for L yields a corresponding value of $J = (37.7 \pm 4.1) \text{ MeV}$, that is entirely consistent with the limit obtained in Eq.(5). Although consistent at the 2σ level, the ‘‘Intersection’’ region in Fig. 2 obtained from a variety of experimental and theoretical approaches lies outside the 1σ PREX-II limits.

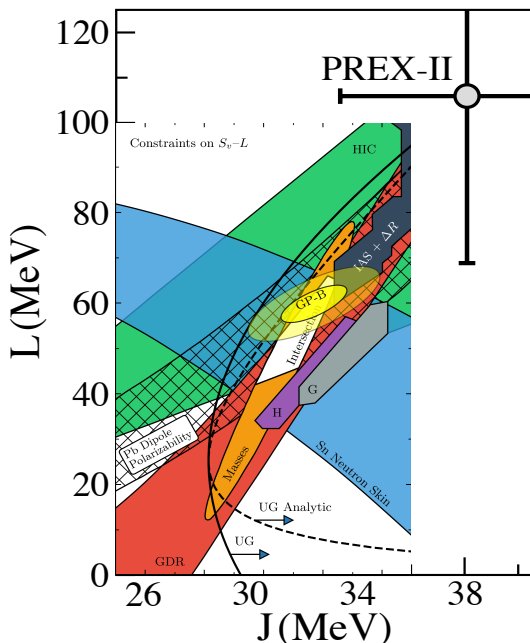


FIG. 2: (Color online). Constraints on the J – L correlation obtained from a variety of experimental and theoretical approaches. The figure was adapted from Refs. [11, 33] and noticeably displays the tension with the recent PREX-II result.

Next, we explore the impact of PREX-II on a few neutron-star observables. We start by displaying in Fig. 3 the minimum central density and associated neutron star mass required for the onset of the direct Urca process. Neutron stars are born very hot ($T \simeq 10^{11} \text{ K} \simeq 10 \text{ MeV}$) and then cool rapidly via neutrino emission through the direct Urca process that involves neutron beta decay followed by electron capture:

$$n \rightarrow p + e^- + \bar{\nu}_e, \quad (7a)$$

$$p + e^- \rightarrow n + \nu_e. \quad (7b)$$

After this rapid cooling phase is completed, neutrino emission proceeds in the standard cooling scenario through the modified Urca process—a process that may

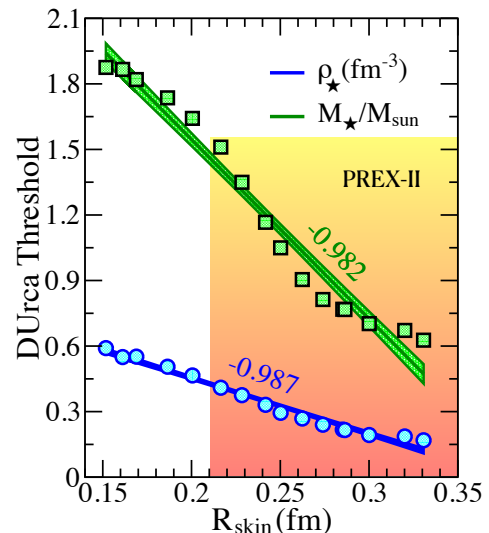


FIG. 3: (Color online). Direct Urca thresholds for the onset of enhanced cooling in neutron stars. The threshold density is depicted by the lower blue line and the corresponding stellar mass for such a central density with the upper green line. The shaded area represents PREX-II 1σ confidence region. For each of these two quantities, the best-fit line is displayed together with their associated correlation coefficients.

be millions of times slower as it requires the presence of a bystander nucleon to conserve momentum at the Fermi surface[34]. The transition into the much slower modified Urca process is solely based on the expectation that the proton fraction in the stellar core is too low to conserve momentum at the Fermi surface. However, given that the proton fraction is controlled by the poorly known density dependence of the symmetry energy [35], the minimal cooling scenario may need to be revisited. In particular, a stiff symmetry energy—as suggested by PREX-II—favors large proton fractions that may trigger the onset of the direct Urca process at lower central densities. This analysis is particularly timely given that x-ray observations suggest that some neutron stars may require some form of enhanced cooling. Indeed, the detected x-ray spectrum of the neutron star in the low-mass x-ray binary MXB 1659-29 strongly suggests the need for a fast neutrino-cooling process [36]. For a comprehensive report that explores the interplay between the direct Urca process and nucleon superfluidity in transiently accreting neutron stars, see Ref. [37]. The shaded area in Fig. 3 displays the region constrained by PREX-II. In particular, the 1σ lower limit of $R_{\text{skin}} = 0.212 \text{ fm}$ suggests a threshold mass for the onset of direct Urca cooling of $M_* \approx 1.45 M_\odot$ and a corresponding central density of $\rho_* \approx 0.42 \text{ fm}^{-3}$. However, if instead one adopts the larger PREX-II central value of $R_{\text{skin}} = 0.283 \text{ fm}$, then one obtains the considerably lower threshold values of $M_* \approx 0.85 M_\odot$ and $\rho_* \approx 0.24 \text{ fm}^{-3}$, or a threshold density just slightly higher than saturation density. Although some stars are likely to require enhanced cooling, observations of many iso-

lated neutron stars are consistent with the much slower modified URCA process [38]. This may be because the direct URCA neutrino emissivity is reduced by nucleon pairing.

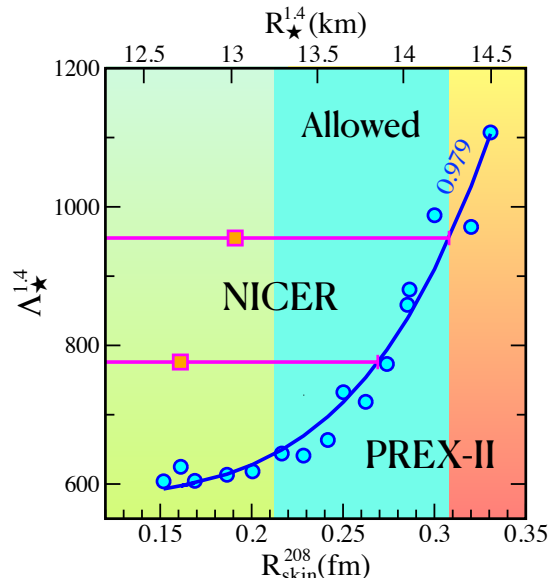


FIG. 4: (Color online). Showcase of neutron star observables as a function of R_{skin}^{208} as predicted by the set of energy density functionals considered in this work. The tidal deformability $\Lambda_{\star}^{1.4}$ of a $1.4 M_{\odot}$ neutron star is computed for each model, and displayed with blue dots and connected by a best fit power law that scales as the $4.8 \approx 5$ power of $R_{\star}^{1.4}$. The combined PREX-II result together with NICER constraints on the stellar radius is depicted by the small (blue) window of models allowed.

We close the section by displaying in Fig. 4 the dimensionless tidal deformability of a $1.4 M_{\odot}$ neutron star as a function of both the stellar radius $R_{\star}^{1.4}$ and R_{skin} . Although not shown, for the set of density functionals used in this work a very strong correlation (of about 0.98) is obtained between $R_{\star}^{1.4}$ and R_{skin} . However, because the central density of a $1.4 M_{\odot}$ neutron star may reach densities as high as 2-to-3 times saturation density, the robustness of such a correlation should be examined in the context of alternative theoretical descriptions. Moreover, a precise knowledge of the EOS of the crust is needed to minimize possible systematic uncertainties [39]. As in Fig. 3, the 1σ confidence region is indicated by the shaded area in the figure. Also shown are NICER constraints on the radius of PSR J0030+0451 [40, 41], that are depicted by the two horizontal error bars and which suggest an upper limit of $R_{\star}^{1.4} \leq 14.26$ km. Invoking the strong $R_{\star}^{1.4} - R_{\text{skin}}$ correlation observed in our models, one obtains an upper limit on the neutron skin thickness of $R_{\text{skin}} \lesssim 0.31$ fm and a lower limit on the stellar radius of $R_{\star}^{1.4} \gtrsim 13.25$ km. The region that satisfies both PREX-II and NICER constraints is indicated by the narrow (blue) rectangle in Fig. 4, which excludes a significant number of models. In turn, given that the tidal deformability approximately scales with the fifth power of the stellar radius [42], one can also set limits on the tidal deformabil-

ity of a $1.4 M_{\odot}$ neutron star. Combining the constraints from NICER on $R_{\star}^{1.4}$ and PREX-II on R_{skin}^{208} one obtains:

$$0.21 \lesssim R_{\text{skin}}(\text{fm}) \lesssim 0.31 \quad (8a)$$

$$13.25 \lesssim R_{\star}^{1.4}(\text{km}) \lesssim 14.26 \quad (8b)$$

$$642 \lesssim \Lambda_{\star}^{1.4} \lesssim 955. \quad (8c)$$

The allowed region for the tidal deformability falls comfortably within the $\Lambda_{\star}^{1.4} \lesssim 800$ limit reported in the GW170817 discovery paper [43]. Yet, the revised limit of $\Lambda_{1.4} = 190_{-120}^{+390} \lesssim 580$ [44] presents a more serious challenge. To confirm whether this tension is real, it will require a multi-prong approach involving a more precise determination of R_{skin}^{208} , additional NICER observations, and more multi-messenger detections of neutron star mergers. The prospect of a more precise electroweak determination of R_{skin}^{208} is challenging as it may require the full operation of the future Mainz Energy-recovery Superconducting Accelerator (MESA) which is foreseen to start until 2023 [45]. Future determinations of stellar radii by NICER for neutron stars with known masses, such as J0437-4715 [46], could be made at a $\pm 3\%$ level, or to better than ± 0.5 km. NICER is also collecting pulse profile modeling data for the highest mass pulsar (PSR J0740+6620) ever measured [47]. Finally, the LIGO-Virgo-KAGRA collaborations are preparing for the fourth observing run at a higher detector sensitivity. Although KAGRA will join LIGO and Virgo promising much better sky localization, COVID-related delays have pushed the fourth observing run until June 2022.

In summary, PREX-II has confirmed with improved precision the original PREX suggestion that the EOS at the typical densities found in atomic nuclei is stiff. This result challenges our present understanding of the density dependence of symmetry energy extracted from various experimental and theoretical analyses [30]. By assessing the impact of PREX-II at higher densities, we were able to provide limits on both the radius and deformability of a $1.4 M_{\odot}$ neutron star. Given that our analysis of the tidal deformability reveals some tension with the revised limit of $\Lambda_{1.4} \lesssim 580$ [44], we eagerly await the next generation of terrestrial experiments and astronomical observations to verify whether the tension remains. If so, the softening of the EOS at intermediate densities, together with the subsequent stiffening at high densities required to support massive neutron stars, may be indicative of a phase transition in the stellar core [42].

Acknowledgments

This material is based upon work supported by the U.S. Department of Energy Office of Science, Office of Nuclear Physics under Awards DE-FG02-87ER40365 (Indiana University), Number DE-FG02-92ER40750 (Florida State University), and Number DE-SC0008808 (NUCLEI SciDAC Collaboration).

-
- [1] S. Abrahamyan, Z. Ahmed, H. Albatineh, K. Aniol, D. S. Armstrong, et al., *Phys. Rev. Lett.* **108**, 112502 (2012).
- [2] C. J. Horowitz, Z. Ahmed, C. M. Jen, A. Rakhman, P. A. Souder, et al., *Phys. Rev.* **C85**, 032501 (2012).
- [3] D. Adhikari et al. (2021), 2102.10767.
- [4] B. A. Brown, *Phys. Rev. Lett.* **85**, 5296 (2000).
- [5] R. J. Furnstahl, *Nucl. Phys.* **A706**, 85 (2002).
- [6] M. Centelles, X. Roca-Maza, X. Viñas, and M. Warda, *Phys. Rev. Lett.* **102**, 122502 (2009).
- [7] X. Roca-Maza, M. Centelles, X. Viñas, and M. Warda, *Phys. Rev. Lett.* **106**, 252501 (2011).
- [8] J. Piekarewicz and M. Centelles, *Phys. Rev.* **C79**, 054311 (2009).
- [9] Z. Zhang and L.-W. Chen, *Phys. Lett.* **B726**, 234 (2013).
- [10] K. Hebeler, J. Lattimer, C. Pethick, and A. Schwenk, *Astrophys. J.* **773**, 11 (2013).
- [11] C. Drischler, R. Furnstahl, J. Melendez, and D. Phillips, *Phys. Rev. Lett.* **125**, 202702 (2020).
- [12] G. Hagen et al., *Nature Phys.* **12**, 186 (2015).
- [13] L.-W. Chen, C. M. Ko, B.-A. Li, and J. Xu, *Phys. Rev.* **C82**, 024321 (2010).
- [14] A. Steiner and S. Gandolfi, *Phys. Rev. Lett.* **108**, 081102 (2012), 1110.4142.
- [15] S. Gandolfi, J. Carlson, S. Reddy, A. Steiner, and R. Wiringa, *Eur. Phys. J.* **A50**, 10 (2014), 1307.5815.
- [16] X. Roca-Maza, X. Viñas, M. Centelles, B. K. Agrawal, G. Colò, N. Paar, J. Piekarewicz, and D. Vretenar, *Phys. Rev.* **C92**, 064304 (2015).
- [17] W.-C. Chen and J. Piekarewicz, *Phys. Rev.* **C90**, 044305 (2014).
- [18] W.-C. Chen and J. Piekarewicz, *Phys. Lett.* **B748**, 284 (2015).
- [19] F. J. Fattoyev and J. Piekarewicz, *Phys. Rev. Lett.* **111**, 162501 (2013).
- [20] J. Piekarewicz, B. Agrawal, G. Colò, W. Nazarewicz, N. Paar, et al., *Phys. Rev.* **C85**, 041302(R) (2012).
- [21] P.-G. Reinhard, J. Piekarewicz, W. Nazarewicz, B. Agrawal, N. Paar, et al., *Phys. Rev.* **C88**, 034325 (2013).
- [22] C. J. Horowitz and J. Piekarewicz, *Phys. Rev. Lett.* **86**, 5647 (2001).
- [23] C. Ducoin, J. Margueron, and C. Providencia, *Europhys. Lett.* **91**, 32001 (2010).
- [24] C. Ducoin, J. Margueron, C. Providencia, and I. Vidana, *Phys. Rev.* **C83**, 045810 (2011).
- [25] C. J. Horowitz, E. F. Brown, Y. Kim, W. G. Lynch, R. Michaels, et al., *J. Phys.* **G41**, 093001 (2014).
- [26] P. Danielewicz, P. Singh, and J. Lee, *Nucl. Phys. A* **958**, 147 (2017).
- [27] A. Trzcińska, J. Jastrzebski, P. Lubiński, F. Hartmann, R. Schmidt, et al., *Phys. Rev. Lett.* **87**, 082501 (2001).
- [28] J. Zenihiro, H. Sakaguchi, T. Murakami, M. Yosoi, Y. Yasuda, et al., *Phys. Rev.* **C82**, 044611 (2010).
- [29] C. Tarbert et al., *Phys. Rev. Lett.* **112**, 242502 (2014).
- [30] M. Thiel, C. Sfienti, J. Piekarewicz, C. J. Horowitz, and M. Vanderhaeghen, *J. Phys.* **G46**, 093003 (2019).
- [31] M. C. Atkinson, M. H. Mahzoon, M. A. Keim, B. A. Bordeon, C. D. Pruitt, R. J. Charity, and W. H. Dickhoff, *Phys. Rev. C* **101**, 044303 (2020).
- [32] C. D. Pruitt, R. J. Charity, L. G. Sobotka, M. C. Atkinson, and W. H. Dickhoff, *Phys. Rev. Lett.* **125**, 102501 (2020).
- [33] J. M. Lattimer, *Ann. Rev. Nucl. Part. Sci.* **62**, 485 (2012).
- [34] D. Page, J. M. Lattimer, M. Prakash, and A. W. Steiner, *Astrophys. J. Suppl.* **155**, 623 (2004).
- [35] C. J. Horowitz and J. Piekarewicz, *Phys. Rev.* **C66**, 055803 (2002).
- [36] E. F. Brown, A. Cumming, F. J. Fattoyev, C. Horowitz, D. Page, and S. Reddy, *Phys. Rev. Lett.* **120**, 182701 (2018).
- [37] A. Potekhin, A. Chugunov, and G. Chabrier, *Astron. Astrophys.* **629**, A88 (2019).
- [38] D. Page, J. M. Lattimer, M. Prakash, and A. W. Steiner, *Astrophys. J.* **707**, 1131 (2009).
- [39] J. Piekarewicz, F. J. Fattoyev, and C. J. Horowitz, *Phys. Rev.* **C90**, 015803 (2014).
- [40] T. E. Riley et al., *Astrophys. J. Lett.* **887**, L21 (2019).
- [41] M. C. Miller et al., *Astrophys. J. Lett.* **887**, L24 (2019).
- [42] F. J. Fattoyev, J. Piekarewicz, and C. J. Horowitz, *Phys. Rev. Lett.* **120**, 172702 (2018).
- [43] B. P. Abbott et al. (Virgo, LIGO Scientific), *Phys. Rev. Lett.* **119**, 161101 (2017).
- [44] B. P. Abbott et al. (Virgo, LIGO Scientific), *Phys. Rev. Lett.* **121**, 161101 (2018).
- [45] D. Becker et al. (2018), 1802.04759.
- [46] D. Reardon et al., *Mon. Not. Roy. Astron. Soc.* **455**, 1751 (2016).
- [47] H. T. Cromartie et al., *Nat. Astron.* **4**, 72 (2019).